Automated interplanetary shock detection and its application to Wind observations

O. Kruparova, M. Maksimovic, J. Šafránková, Z. Němeček, O. Santolík, V. Krupar

JOURNAL OF GEOPHYSICAL RESEARCH: SPACE PHYSICS, VOL. 118, 4793–4803, doi:10.1002/jgra.50468, 2013

Automated interplanetary shock detection and its application to Wind observations

O. Kruparova,[1] M. Maksimovic,[2] J. Šafránková,[3] Z. Němeček,[3]
O. Santolik,[1,3] and V. Krupar[1]

Received 29 October 2012; revised 12 July 2013; accepted 21 July 2013; published 26 August 2013.

[1] We present an automated two-step detection algorithm for identification of interplanetary (IP) shocks regardless their type in a real-time data stream. This algorithm is aimed for implementation on board the future Solar Orbiter mission for triggering the transmission of the high-resolution data to the Earth. The first step of the algorithm is based on a determination of a quality factor, Q indicating abrupt changes of plasma parameters (proton density and bulk velocity) and magnetic field strength. We test two sets of weighting coefficients for Q determination and propose the second step consisting of three additional constraints that increase the effectiveness of the algorithm. We checked the algorithm using Wind (at 1 AU) and Helios (at distances from 0.29 to 1 AU) data and compared obtained results with already existing lists of IP shocks. The efficiency of the presented algorithm for the Wind shock lists varies from 60% to 84% for two Q thresholds. The final shock candidate list provided by the presented algorithm contains the real IP shocks, as well as different discontinuities. The detection rate of the IP shocks equals to 64% and 29% for two Q thresholds. The algorithm detected all IP shocks associated with the solar wind transient structures triggering intense (Dst < –100 nT) geomagnetic storms.

Citation: Kruparova, O., M. Maksimovic, J. Šafránková, Z. Němeček, O. Santolik, and V. Krupar (2013), Automated interplanetary shock detection and its application to Wind observations, *J. Geophys. Res. Space Physics*, *118*, 4793–4803, doi:10.1002/jgra.50468.

1. Introduction

[2] Interplanetary (IP) shocks are formed in the solar wind as precursors of the arrival of large transient structures of solar origin due to nonlinear effects [*Tsurutani et al.*, 1988; *Tsurutani et al.*, 2011]. They are generated by the interaction of fast and slow solar wind streams (specifically at the boundaries of corotating interaction regions, CIRs) and by the passage of transient phenomena such as Coronal Mass Ejections (CMEs) propagating through the interplanetary medium [e.g., *Luhmann*, 1997] as Interplanetary Coronal Mass Ejections (ICMEs).

[3] Solar Orbiter was selected as one of the missions within the European Space Agency Cosmic Vision 2015–2025 programme [*Müller et al.*, 2012]. Following the launch scheduled for January 2017, the Solar Orbiter spacecraft will orbit the Sun at distances reaching 0.28 AU by the end of the mission. The spacecraft will carry a payload including the remote sensing instruments tasked to monitor the dynamics of the Sun and its surface layers and the *in situ* instruments, which will study the particles, fields, and waves in the solar wind immediately above the remotely observed source regions. The payload is suitable to register IP shocks together with their drivers; therefore, it may significantly contribute to our further understanding of shock formations, their fine structure, and a connection with a particular driver [*March et al.*, 2005], but these tasks require high-time resolution measurements. The present experimental techniques can provide the data with a sufficient time resolution, but data transmission rates allow only a limited sample of such data to be returned to the Earth.

[4] One of the possible solutions is a trigger system operating onboard Solar Orbiter that would analyze data, select predetermined events according to the specified criteria, and transmit an identified sample of the data with the highest time resolution to the Earth.

[5] This idea is not new; the first algorithm for IP shock detection based on magnetic field measurements was applied on Helios-1 and Helios-2 [*Musmann et al.*, 1979]. The Helios automated event detector continuously computed the quality index A from a relative change of the squared magnetic field magnitude and compared short-time mean values with long-time mean values. Due to the memory shortage, this algorithm stored high-time resolution data for the event with the highest quality index between two telemetry

[1]Institute of Atmospheric Physics, the Academy of Sciences of the Czech Republic, Prague, Czech Republic.
[2]Laboratoire d'Etudes Spatiales et d'Instrumentation en Astrophysique—UMR CNRS 8109, Observatoire de Paris, Meudon, France.
[3]Faculty of Mathematics and Physics, Charles University, Prague, Czech Republic.

Corresponding author: O. Kruparova, Institute of Atmospheric Physics, Czech Academy of Science, Bocni II 1401, 141 31 Prague, Czech Republic. (ok@ufa.cas.cz)

2169-9380/13/10.1002/jgra.50468

sessions. However, the described algorithm was extremely sensitive to short-time fluctuations of the magnetic field that led to a great number of false IP shock detections or to registration of other solar wind discontinuities. Similar IP shock detection systems were developed later for the Intershock [*Galeev et al.*, 1986] and ISEE [*Joselyn et al.*, 1981] spacecraft.

[6] Recent space missions, Wind and ACE operating in the solar wind near the L1 point, are not equipped with IP shock detection systems because the telemetry rate allows to transmit a whole data set with sufficient time resolutions. A complex burst mode trigger is working onboard the STEREO spacecraft. It combines eight individual criteria from several instruments with different weighted components [*Luhmann et al.*, 2008]. At the beginning of the spacecraft operation, the algorithm involved the changes of the following parameters: the magnetic field vector, electron, superthermal electron and proton density fluxes, and electric field fluctuation power in several frequency bands. Since the spacecraft launch, the trigger was continuously modified in order to optimize its criteria for maximum algorithm effectiveness; some of the components were disabled. The success rate of the algorithm changed from 30% in 2007 to 69% in 2011 [*Jian et al.*, 2013]. However, this burst mode trigger is rather complicated and cannot be easily implemented into other missions.

[7] Other IP shock "searching" algorithms based on different identification approaches, e.g., MHD approach, wavelet analysis, or generalized minimum variance analysis were proposed by *Vandev et al.* [1986] and *Kartalev et al.* [2002]. However, such algorithms are only suitable for analyses on the ground.

[8] Furthermore, there are several web applications with near real-time detectors that perform data analysis and select the possible shock candidates. IPS-SWS-ALERT (http://www.ips.gov.au) is an automated experimental product for the ACE data processing, and Shockspotter routines use data from the CELIAS/MTOF/PM sensor on the SOHO spacecraft (http://umtof.umd.edu/pm/). *Vorotnikov et al.* [2008, 2011] presented a fully automated code applied to the ACE data that selects upstream and downstream reference points, computes the shock normal, analyzes IP shocks using Rankine-Hugoniot jump conditions, and provides their solutions for real-time space weather applications. This shock-finder is able to find up to 40% of all manually identified shocks, and this rate increases to 67% with interactive solutions.

[9] The development of such automated procedures for an identification of various structures could also contribute to a space weather warning system and space weather forecasting. It has been shown that fast forward IP shocks and the enhanced plasma densities downstream [*Kennel et al.*, 1985] rapidly compress the magnetosphere after their impact [e.g., *Echer et al.*, 2006; *Tsurutani et al.*, 2011]. The structures associated with or driving the shocks can sometimes trigger intense geomagnetic storms, but the preconditioning of the magnetosphere is an important factor [*Zhou and Tsurutani*, 2001] for such process.

[10] A strong association has been observed between ICMEs sheaths and IP shocks [*Watari and Watanabe*, 1998; *Tsurutani et al.*, 1988; *Lindsay et al.*, 1994], between IP shocks and magnetic clouds [*Lepping et al.*, 2001; *Luhmann*, 1997], and between IP shocks and resulting geomagnetic disturbances [*Gonzalez et al.*, 1999; *Tsurutani et al.*, 1992; *Tsurutani and Gonzalez*, 1998].

[11] One of important recent experimental results is that features of magnetic storms/substorms depend on the type of the interplanetary driver [*Gonzalez et al.*, 1994; *Tsurutani et al.*, 2006]. Therefore, the capability to forecast such events is critical to a successful prediction of space weather. IP shocks in front of potential storm drivers can be easily identified in interplanetary data by solar wind monitors at 1 AU, therefore, they serve as input data into numerical models that forecast the geomagnetic activity [*Tóth et al.*, 2005; *McKenna-Lawlor et al.*, 2006; 2012].

[12] In the paper, we present a simple and flexible algorithm that indicates the possible IP shock arrival. This onboard algorithm is designed for application in the Radio and Plasma Waves (RPW) instrument [*Maksimovic et al.*, 2007] for Solar Orbiter. It is based on interplanetary magnetic field and plasma measurements. The algorithm would allow us to register possible shocks in the solar wind from a beginning phase of the mission as well as at smaller distances from the Sun. Since a whole mission is long, the algorithm should reflect the variations of solar activity. The main task of the suggested algorithm is to identify all types of IP shocks (fast/slow and forward/reverse) regardless of their drivers, but it should exclude the events corresponding to abrupt large increases/decreases of plasma densities that are not associated with IP shocks [*Zastenker et al.*, 2006].

[13] The algorithm development is based on Wind measurements covering the half of the solar cycle 23, and the results are tested against IP shocks identified by other methods. We applied the suggested algorithm on a list of IP shocks observed by Wind that was compiled by J. C. Kasper. The list is available on web (http://www.cfa.harvard.edu/shocks/), and we call it as "Kasper's list" throughout the paper. The test of the algorithm effectiveness in different distances from the Sun is based on the list of IP shocks observed by Helios between 0.29 and 1 AU [*de Lucas et al.*, 2011].

2. Shock Detection Algorithm

[14] IP shocks are observed as abrupt changes of plasma parameters (solar wind speed, temperature, and density) and the magnetic field strength. The sense of such jumps (positive and negative) differs according to the IP shock type. The properties of the different types of shocks are referred e.g., in *Kennel et al.* [1985] and *Tsurutani et al.* [2011].

[15] The first step of our automated identification of the IP shocks is based on detection of simultaneous jumps of the density, velocity, and magnetic field strength. Since we do not focus on a particular type of IP shocks, we use the magnitude of parameter jumps in the first step. The positive sense of the velocity jump that is obligatory across IP shocks will be incorporated into the second step of the algorithm. The sign of variations of the magnetic field and density could be used for the additional analysis of the shock type, but this is not a part of the present algorithm. Slow and reverse shocks [*Ho et al.*, 1998; *Lin et al.*, 2009] are rather rare in the solar wind (see e.g., the Kasper's list). It means that these shocks would not significantly increase the volume of the transmitted data. On the other hand, these shocks are understood in a much lesser extent than the fast forward shocks and

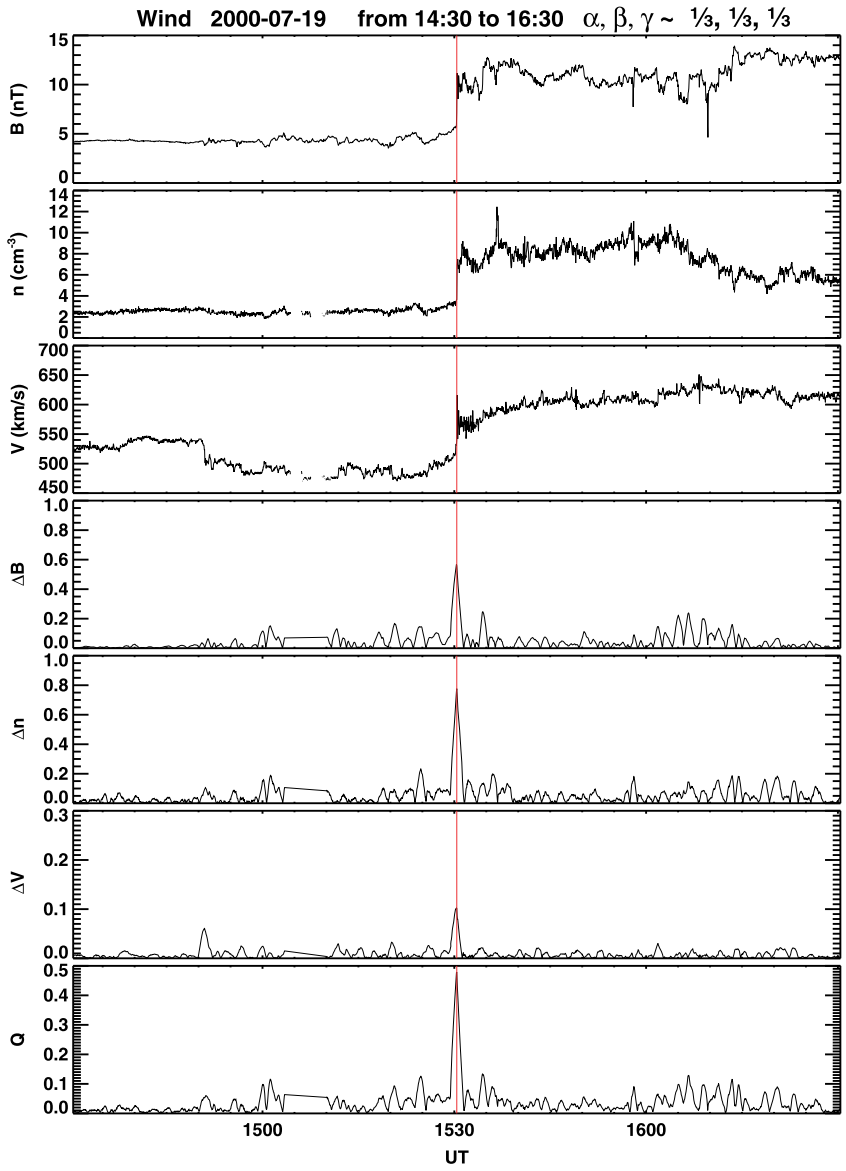

Figure 1. An example of the quasi-perpendicular shock observed by Wind on 19 July 2000. The panels represent the magnetic field magnitude B, the proton density n, proton flow velocity V, ΔB, Δn, ΔV, and quality factor Q with coefficients $\alpha, \beta, \gamma = \frac{1}{3}$. The vertical red line denotes to the shock mark made by automated shock detection algorithm.

the high-resolution data are desirable for their investigation. It should be noted that the details of shocks such as their normal angles relative to the upstream magnetic field and the Mach number are not included into the algorithm. This analysis will be done on the ground using more sophisticated fitting techniques, but the plasma density and magnetic field jump conditions will be given.

[16] The detection algorithm continuously evaluates a quality factor Q that is based on changes of moving averages of several solar wind parameters over a time interval corresponding to a typical IP shock scale. If we expect a sliding window with a width ΔT centered at the time t, the quality factor can be defined as

$$Q = \alpha \Delta B + \beta \Delta n + \gamma \Delta V, \tag{1}$$

$$\alpha + \beta + \gamma = 1, \tag{2}$$

$$\Delta B = \frac{2 \mid B_2 - B_1 \mid}{B_2 + B_1}, \tag{3}$$

$$\Delta n = \frac{2 \mid n_2 - n_1 \mid}{n_2 + n_1}, \tag{4}$$

$$\Delta V = \frac{2 \mid V_2 - V_1 \mid}{V_2 + V_1}, \tag{5}$$

where the magnetic field magnitude B, proton density n, and proton flow velocity V with 1 and 2 subscripts standing for mean values calculated on $[t - \frac{\Delta T}{2}, t]$ and $[t, t + \frac{\Delta T}{2}]$ time intervals, respectively. The time interval of averaging $\frac{\Delta T}{2}$ can be considered as a free parameter of the detection algorithm. Coefficients α, β, and γ denote weights of the parameters ΔB, Δn, and ΔV. The proton temperature could be also included as an additional input parameter since it

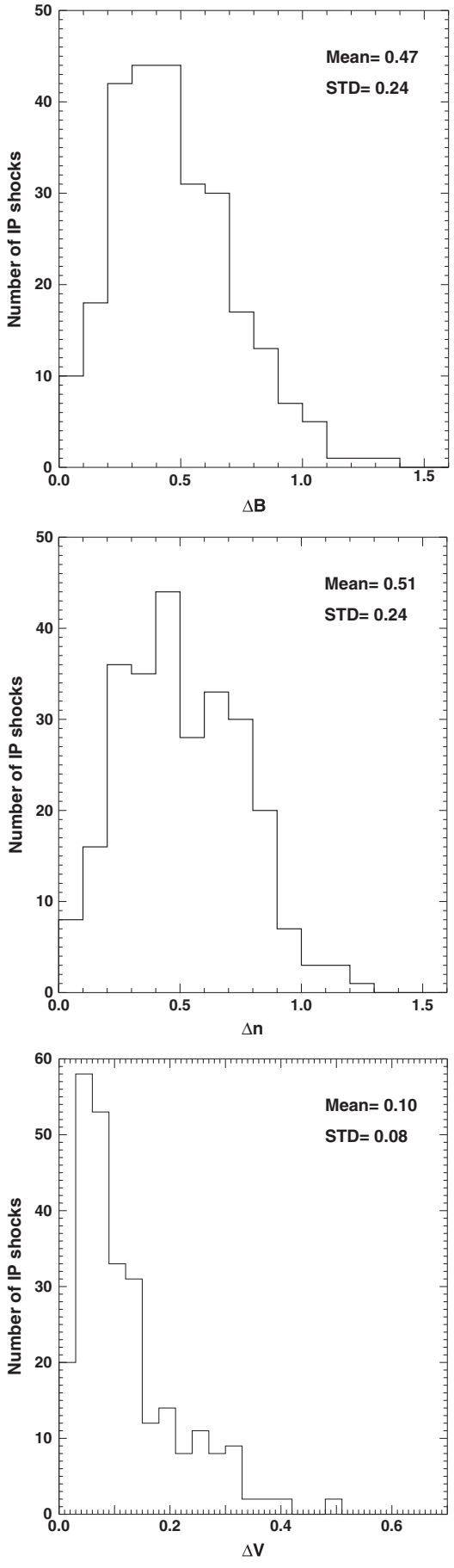

should exhibit a significant jump at the shock. However, the proton temperature is the most uncertain plasma parameter because a determination of the temperature requires careful processing of the full 3-D distribution. Simplified versions of onboard algorithms for computation of plasma moments do not provide reliable temperature data in highly disturbed plasma upstream and downstream of a shock.

[17] An example of the quasi-perpendicular shock (i.e., the θ_{Bn} angle between the shock normal and upstream magnetic field is $> 45°$) detected on 19 July 2000 at 1530 UT by the Wind spacecraft together with the continuously computed quality parameter Q is presented in Figure 1. Normalization coefficients α, β, and γ are equal to one third $\left(\alpha, \beta, \gamma = \frac{1}{3}, \frac{1}{3}, \frac{1}{3}\right)$ in this particular case. Each data point of Q, ΔB, Δn, and ΔV is calculated according to equations (1–5), and we use $\frac{\Delta T}{2} = 5$ min throughout the paper. The quality factor Q shows a significant enhancement at the shock front (vertical red line) and such shock is recorded by the detection algorithm.

3. Quality Factor Evaluation

[18] Our analysis is based on 266 shocks from years of 1995 to 2002, i.e., during the first half of the solar cycle 23 that are listed in the Kasper's list. However, it should be noted that the list is not complete and some IP shocks observed within this time interval are not listed. For the quality factor evaluation as well as for the further statistical analysis, we processed high-resolution plasma moments (3 s) computed onboard by the 3DP instrument [*Lin et al.*, 1995] and 3 s magnetic field by Magnetic Fields Investigation [*Lepping et al.*, 1995] on time intervals when Wind was located in the solar wind.

[19] Figure 2 displays the histograms of ΔB, Δn, and ΔV maxima near the shocks from the Kasper's list. The mean value of ΔV is small (0.1) in a comparison with the other two parameters ΔB and Δn that are 0.47 and 0.51, respectively. *Vorotnikov et al.* [2008] found that the weakest shocks visually identified in the 1999 ACE data plots exhibit 1.5% jumps in the velocity, while 20% jumps in the proton density were observed. The distribution of changes of plasma and magnetic field parameters across IP shocks during solar maximum and minimum presented by *Echer et al.* [2003] demonstrates that a compression ratio is higher for the density (2.60 ± 1.10) than for the magnetic field (1.97 ± 0.57). All these results are in a general agreement and suggest that the normalization coefficients would not be equal.

[20] In order to balance the influence of the input parameters, we strengthen a weight of velocity variations because the velocity jump is one of the principal characteristics of IP shocks, while weights of other two parameters would be smaller. Typical values of ΔB and Δn are comparable but *Zastenker et al.* [2006] have shown that density structures with sharp boundaries traveling with the solar wind are rather frequent. For this reason and based on the above mentioned *Echer et al.* [2003] analysis, we depress the influence of the density jump on the Q value and use the following combination of weight coefficients: $\alpha, \beta, \gamma = \frac{1}{4}, \frac{1}{12}, \frac{2}{3}$.

Figure 2. Histograms of the ΔB, Δn, ΔV parameters calculated for the IP shocks from the Kasper's list.

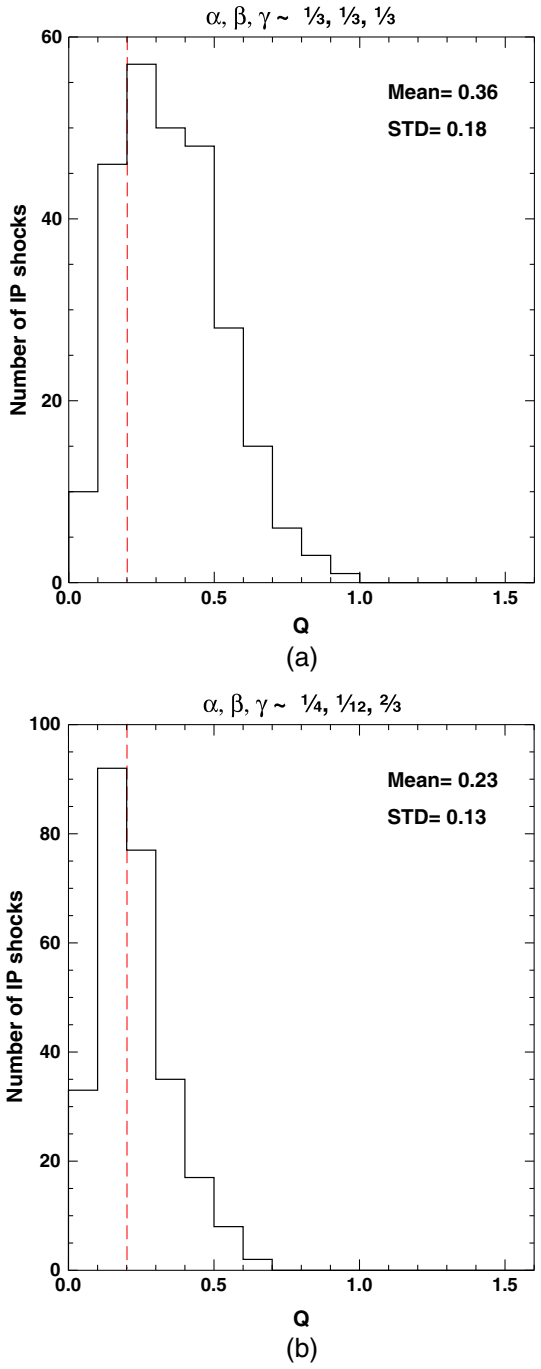

Figure 3. Histograms of the quality factor Q for two sets of α, β, and γ weighting coefficients: (a) set A, (b) set B. The red lines correspond to the threshold $Q = 0.2$.

[21] We plot the distributions of Q for two sets of α, β, and γ coefficients for the shocks in the Kasper's list in Figure 3. Figure 3a uses equal values of coefficients of $\frac{1}{3}$, whereas the values of $\frac{1}{4}$, $\frac{1}{12}$, and $\frac{2}{3}$ are applied in Figure 3b. Hereinafter, we will call the former set "set A" and the latter one "set B".

[22] As it could be expected, an application of nonequal coefficients (set B) leads to decrease of the Q mean value from 0.36 to 0.23. The red dashed lines in both histograms stand for $Q = 0.2$ that was preliminarily chosen as a threshold for the shock identification. Figure 3 shows that 208 of 266 shocks (78%) pass this criterion for the set A but this number decreases to 165 (62%) for the set B. These numbers apparently suggest that the set A would be more appropriate for the shock identification but the percentage of shocks already identified by other methods and passing our threshold cannot be the unique criterion because the algorithm will be applied on the continuous data stream. Thus, the number of nonshock events that pass the threshold would be equally important.

[23] To test the algorithm performance on the real solar wind data, we applied the detection algorithm with the threshold $Q = 0.2$ and two aforementioned sets of weighting coefficients α, β, and γ on 1 month of the Wind data (May 2002). There are six IP shocks in the Kasper's list during this time interval, all of them passed the threshold $Q = 0.2$ for both A and B sets. The results of this test revealed 105 events that passed the threshold $Q = 0.2$ for the set A and that could be the potential shock candidates. A similar number for the set B was 30. These numbers of shock candidates contain real IP shocks as well as false events that also fulfilled our conditions. It means that the set B can be considered as more effective since it rapidly reduces the number of the false candidates.

4. Additional Constraints

[24] The automated shock detection algorithm would identify as much real shocks as possible, however, with a minimum number of false alarms. Therefore, we added some additional requirements with motivation to further decrease a number of shock candidates. Table 1 contains the list of these additional constraints. Our procedures are as follows. For an initial selection of the shock candidates, we use a threshold of the quality factor Q as a first condition that is flexible and may control the number of the detected IP shock candidates. These candidates correspond to the local maxima of the quality factor above a basic threshold. In the second step, we test the remaining candidates with respect to their values of ΔB, Δn, and ΔV. The candidates with relative differences smaller than at least one of the thresholds are rejected. The full definition of this constraint is in Table 1. After the application of the second constraint, the number of shock candidates decreased to $\sim$ 70%. The third constraint characterizes the velocity jump. Since the solar wind velocity increases across all types of IP shocks [*Gosling et al.*, 1994; *Manchester and Zurbuchen*, 2006], we expect $V_2 > V_1$ and the candidates with the negative velocity jump are discarded.

[25] The fourth constraint excludes the different types of discontinuities and fluctuations in the magnetic field and plasma parameters that are not associated with IP shocks. Since IP shocks are rarely parallel (see section 6), one would expect similar relative jumps of ΔB and Δn, thus we discard those candidates with large differences of B and n compression ratios from the list. This condition would also remove density structures reported by *Zastenker et al.* [2006].

[26] As we already noted, the shocks observed in May 2002 passed the threshold $Q = 0.2$ but the analysis of all shocks from the Kasper's list has shown that the threshold of 0.2 seems to be too restrictive (see Figure 2). Since we introduced the additional constraints, we can decrease the value of Q to 0.12. This value and the additional constraints

Table 1. List of Basic and Additional Constraints

1.	$Q >$ (Flexible threshold)	The basic condition for the shock candidate selection
2.	$\Delta B > 0.1$ and $\Delta n > 0.1$ and $\Delta V > 0.03$	Reject shock candidates with weak changes of plasma parameters and magnetic field strength
3.	$V_1 > V_2$	Reject shock candidates with a negative jump of the velocity
4.	$\lvert\Delta B - \Delta n\rvert < 0.3$ or $\Delta V > 0.1$	Reject candidates with very different compression ratios of B and n

were applied on all 266 IP shocks from the Kasper's list. The results are demonstrated in Figure 4. The full circles stand for the shocks that exhibit the quality factor above the threshold, and velocity jumps are indicated by their color. The 238 shocks passed the threshold $Q = 0.12$ and 14 of them were excluded by our additional constraints. We can note that 165 of 266 shocks passed the threshold of $Q = 0.2$, and six events were discarded later by the additional constraints.

[27] A detailed investigation of the 28 undetected shocks from the Kasper's list with the quality factor under 0.12 showed that the main reason is a small velocity jump, i.e., less than 25 km/s (15 cases) or an insignificant change of the magnetic field strength (2–4 nT) for the remaining cases.

[28] A further analysis revealed that constraint number four (see Table 1) removed predominantly slow forward and quasi-parallel shocks. A demonstration of the application of this constraint can be found in Figure 5, which shows an example of three IP shocks detected on 11 April 2001. All presented shocks exhibit sufficient Q but one event (indicated by the black cross in Figure 5) was discarded by constraint number four. This shock exhibits a strong decrease of the magnetic field in contrast to a small increase of the proton density, and therefore, the difference $|\Delta B - \Delta n|$ exceeds the threshold of 0.3 in the fourth constraint. The presented event was classified as a slow forward IP shock in the Kasper's shock list but we should note that the proper reason for its discarding was a large difference between ΔB and Δn, not the shock type.

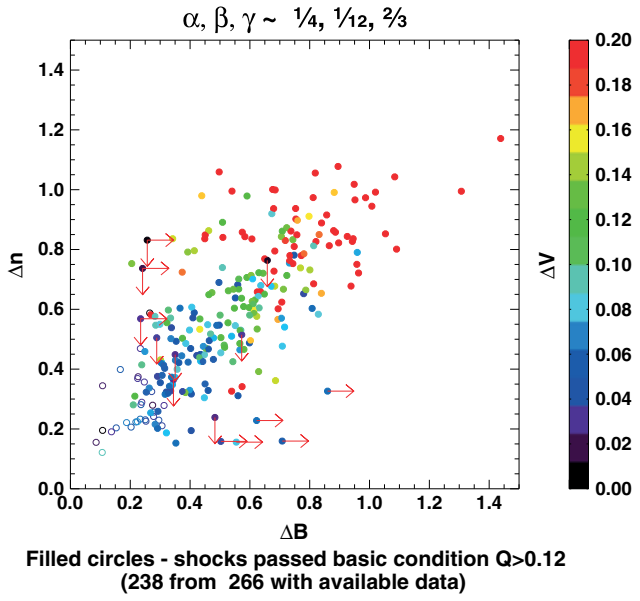

Figure 4. Demonstration of the algorithm efficiency applied on the Kasper's shock list. All shocks are presented as the empty circles with the color corresponding to the values of ΔV. Filled circles display the number of the shock events passed the basic condition, i. e., Q threshold. Red arrows display the shocks excluded by the additional constraints (downward arrows—second constraint, rightward arrows—fourth constraint).

5. Statistical Evaluation of the Shock Detection

[29] To evaluate our algorithm, we have applied it on 8 years of the continuous Wind measurements that are covered by the Kasper's shock list. The results are summarized in Table 2 for $Q = 0.2$ and in Table 3 for $Q = 0.12$. In both tables, the first line shows the number of initial shock candidates that passed the given quality threshold. The lines denoted by 2–4 indicate the numbers of shock candidates remaining after application of the corresponding additional constraint (described in Table 1).

[30] The line denoted as "Final shock candidates" contains a number of shock candidates after the four-step reduction procedure. We have checked all these candidates by a visual inspection of magnetic field and plasma parameter plots. The number of "real" IP shocks that were identified by this way together with the corresponding success rate (in percents) is shown in the next two lines. Finally, the following lines show the number of shocks that can be found in the Kasper's list for a particular year and the number of those passing our detection algorithm.

[31] As it can be seen from a comparison of Tables 3 and 2, a decrease of the threshold Q leads to the increase of the number of detected shocks as well to the increase of the number of shock candidates. The efficiency of our algorithm applied to the Kasper's list improved from 60% to 84% by decreasing the Q threshold from 0.2 to 0.12. However, the number of shock candidates increased more than three times (from 312 to 1056).

[32] As it was mentioned above, the Kasper's list is far from being complete and there are many shocks that are not listed there. We have examined the final shock candidates for both 0.2 and 0.12 Q thresholds and found 40 and 86 additional shocks not included in the Kasper's list, respectively. The final detection rate of the shocks was 29% for the quality factor of 0.12 and 64% for $Q = 0.2$.

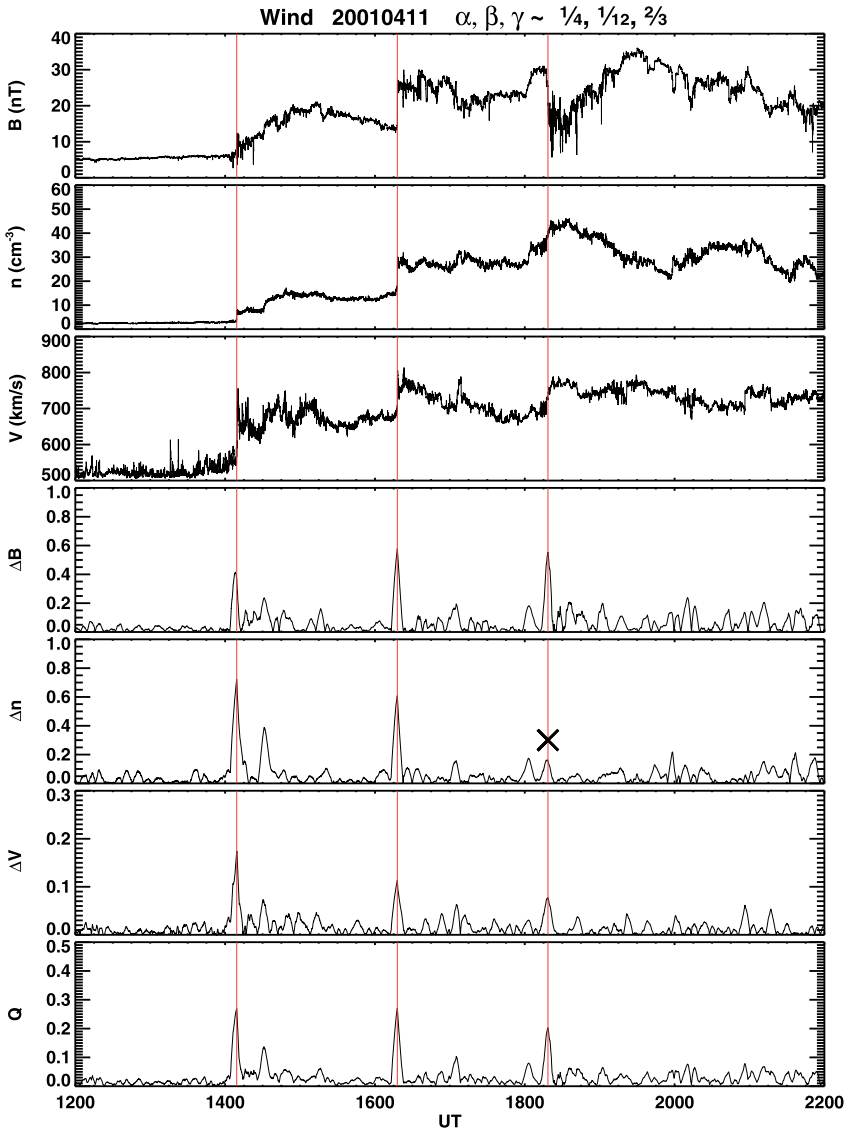

Figure 5. An example of IP shocks passage observed by Wind on 11 April 2001. The panels represent the magnetic field magnitude B, the proton density n, proton flow velocity V, ΔB, Δn, ΔV, and quality factor Q. The vertical red lines denote to the shock mark made by automated shock detection algorithm. The black cross corresponds to the event discarded by the additional constraint.

Table 2. Detailed Results of the Blind Test Made on 8 Years of the Wind Data With the Q Threshold 0.2 and With the Coefficients α, β, and γ Equal to $\frac{1}{4}$, $\frac{1}{12}$, and $\frac{2}{3}$, Respectively

	Solar Minimum				Solar Maximum				
	1995	1996	1997	1998	1999	2000	2001	2002	Total
Constraint 1 ($Q > 0.2$)	622	354	313	244	205	259	275	146	2418
Constraint 2	60	74	80	82	79	104	95	64	638
Constraint 3	35	48	50	60	52	76	74	49	444
Constraint 4	23	15	32	43	40	57	61	41	312
Final shock candidates	23	15	32	43	40	57	61	41	312
"Real" shocks	11	6	19	25	24	38	42	34	199
% of "real" shocks	48%	40%	59%	58%	60%	67%	69%	83%	64%
Shocks in Kasper's list	20	18	29	26	27	39	70	37	266
Detected Kasper's shocks	9	2	14	21	20	29	41	23	159
% of detected Kasper's shocks	45%	11%	48%	80%	74%	74%	58%	62%	60%

Table 3. Detailed Results of the Blind Test Made on 8 Years of the Wind Data With the Q Threshold of 0.12 and With the Coefficients α, β, and γ Equal to $\frac{1}{4}$, $\frac{1}{12}$, and $\frac{2}{3}$, Respectively

	Solar Minimum				Solar Maximum				
	1995	1996	1997	1998	1999	2000	2001	2002	Total
Constraint 1 ($Q > 0.12$)	1721	2000	1618	1176	920	1095	1184	712	10426
Constraint 2	275	324	272	296	239	278	281	207	2172
Constraint 3	154	189	171	180	154	177	189	139	1353
Constraint 4	120	126	132	143	131	136	153	115	1056
Final shock candidates	120	126	132	143	131	136	153	115	1056
"Real" shocks	20	15	34	34	38	53	66	50	310
% of "real" shocks	17%	12%	26%	24%	29%	39%	43%	43%	29%
Shocks in Kasper's list	20	18	29	26	27	39	70	37	266
Detected Kasper's shocks	14	11	26	23	24	36	58	32	224
% of detected Kasper's shocks	70%	61%	89%	88%	88%	92%	82%	86%	84%

6. Discussion

[33] While developing the presented algorithm, we looked for an optimal relation between the identified real IP shocks and the false candidates. There are several flexible input parameters that can change the output number of shock candidates according to the user's needs:

[34] 1. The time interval ΔT for ΔB, Δn, and ΔV computation is the first parameter regulating the algorithm sensitivity to small fluctuations of data which in turn controls the initial number of shock candidates. For our statistical study, we used 5 min mean values ($\Delta T = 10$ min) that are sufficient for identification of even weak IP shocks and that ignore short-time disturbances.

[35] 2. The second regulating parameter is the set of weighting coefficients α, β, and γ. Their values can change the influence of the separate inputs (B, n, and V) on the quality factor and regulate the output number of shock candidates.

[36] 3. The constraints presented in Table 1 are the additional regulating mechanism that can be adjusted to the current solar wind conditions, e.g., to the solar cycle phase.

[37] In previous sections, we demonstrated the performance of the IP shock detection algorithm on the data from Wind that operates near the L1 point. Since Solar Orbiter would approach ≈0.3 AU where the solar wind characteristics are different, we checked the performance of our algorithm using the data collected closer to the Sun. Considering the spacecraft orbit, Helios observations seems to be the most appropriate for testing, since they cover almost whole inner heliosphere from 0.28 to 1 AU. As a reference shock list, we used database compiled by *de Lucas et al.* [2011] that is available on web http://www.dge.inpe.br/maghel/EN/index.html. The list presents 395 shocks detected by both spacecraft during Solar Cycle 21 from 1974 to 1986, but only for 250 of them we have plasma and magnetic field data simultaneously.

[38] The solar wind parameters vary with the heliocentric distance except of the solar wind bulk speed that remains almost unchanged. Figure 6 shows the histograms of ΔB, Δn, and ΔV calculated from upstream and downstream averaged values available also in the *de Lucas et al.* [2011] database. We divided the Helios shock list into two subsets according to the heliocentric distance: 0.29–0.7 AU (black histogram) and 0.7–1 AU (red histogram). One can see that the mean value of ΔV decreases from 0.21 to 0.16 with the heliocentric distance, whereas the other two parameters ΔB and Δn remain nearly unchanged. We can conclude that our algorithm would be sufficient even in closest approach of the Sun by Solar Orbiter.

[39] The performance of our simple algorithm is fully comparable with the sophisticated trigger working currently onboard STEREO. According to *Jian et al.* [2013], the performance rate of the STEREO algorithm increased from 30% to 69% in course of the 2007–2011 years. The authors attribute this increase to several changes of the weighting factors but we think that this increase can be partly connected with increasing solar activity. The similar apparent enhancement of the performance rate of our simple algorithm from the solar minimum to maximum is clearly seen in Tables 2 and 3.

[40] The algorithm would detect better quasi-perpendicular IP shocks because they exhibit significant jumps of the input parameters in contrast to quasi-parallel shocks. The regions upstream and downstream of quasi-parallel shocks are populated by energized ions that complicate the determination of plasma moments by simple onboard codes [*Tsurutani and Lin*, 1985]. Turbulence that is predominantly visible in the magnetic field profile leads to a formation of islands where the amplitudes of all parameters often exceed their downstream values [*Schwartz*, 2006]. Averaging over 5 min that is a part of our algorithm filters these fluctuations, and the resulting profile exhibits usually gradual changes and thus Q is low. Moreover, our second and fourth constraints expect significant jumps of the magnetic field across the shock but the magnetic field is unchanged at a strictly parallel shock. On the other hand, the histogram in Figure 7 where the number of shocks from the Kasper's list is plotted as a function of the θ_{Bn} angle suggests that parallel or quasi-parallel IP shocks are rather rare. We do not speculate if the lack of quasi-parallel shocks that follows from Figure 7 is real or if it is apparent and caused by above discussed difficulties with their clear identification. We can only note that the effectiveness of the identification of the shocks from the Kasper's list does not depend on the θ_{Bn} significantly.

[41] The detection algorithm would be more effective for fast shocks because the compression of the magnetic field and density is larger for them in comparison with slow shocks. The success rates of identification of slow and fast shocks from the Kasper's list were similar. We think that the above discussion about difficulties with quasi-parallel shock

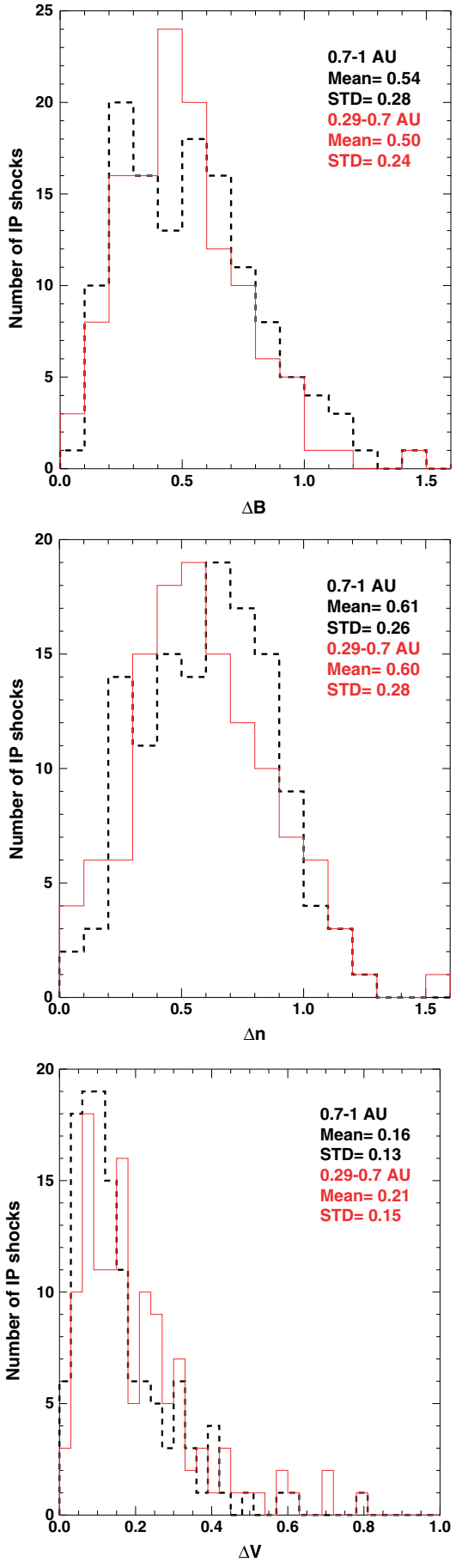

Figure 6. Histograms of ΔB, Δn, and ΔV parameters calculated for the shocks from the Helios shock list.

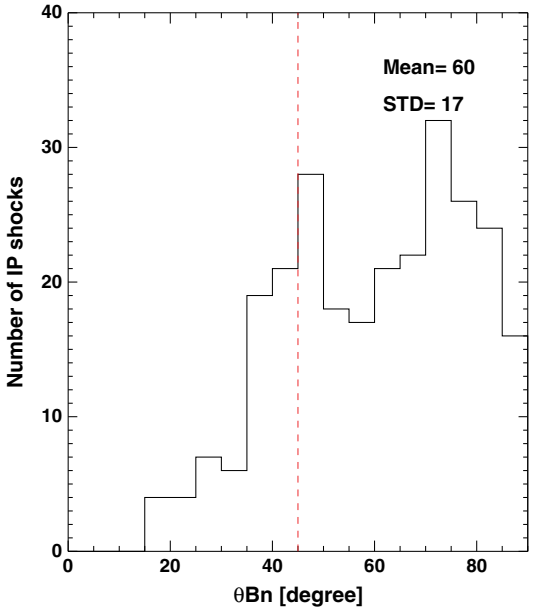

Figure 7. Histogram of the θ_{Bn} for the shocks from the Kasper's list. The red dashed line corresponds to $\theta_{Bn} = 45°$.

identification can be applied on the slow shocks too. It is natural that the algorithm works better for strong shocks but it is able to identify even very weak shocks with a clear structure. For example, a shock with $\Delta V \approx 0.07$, $\Delta B \approx 0.3$, and $\Delta n \approx 0.4$ is really weak but it will be found because its $Q = 0.15$ and additional constraints are satisfied.

[42] Although the algorithm is primarily designed for onboard IP shock identification, it can be used for purposes of space weather as well. For this application, the geoeffectiveness of the identified/missed structures would be the most important parameter. We have tested the geomagnetic activity following the IP shocks from the Kasper's list and found that none of the events undetected by the presented algorithm (regardless of the quality factor value) triggered geomagnetic storms. Also, the IP shocks discarded by the additional constraints were not geoeffective. It means that the algorithm did not miss any IP shock important for the space weather prediction.

7. Conclusion

[43] We have described an automated two-step shock detection algorithm that can be easily adapted for a real-time IP shock identification onboard the spacecraft or as the IP shock alert suitable for space weather studies. We have applied it to the magnetic field and plasma data from the Wind spacecraft. The detection rate can be regulated via a flexible threshold of the quality factor Q. Applying the fully automated code on science-quality level 2 data of the Wind spacecraft for the years of 1995–2002, we found 60% and 84% of all shocks from the Kasper's list using Q equal to 0.2 and 0.12, respectively. The suggested algorithm identifies better quasi-perpendicular IP shocks, since all parameters change abruptly in contrast to the quasi-parallel cases.

[44] The final shock candidate list contains the real IP shocks as well as the false events corresponding to strong fluctuations of plasma parameters and magnetic field or other discontinuities. The final detection rate of the IP shocks found by our algorithm equals to 64% and 29% for Q thresholds of 0.12 and 0.2, respectively.

[45] We tested our algorithm on the Helios data and confirmed the efficiency of the algorithm and suitability of the selection of coefficients α, β, and γ at different heliocentric distances regardless of plasma and magnetic field variations.

[46] We have analyzed the geoeffectiveness of the non-identified shocks from the Kasper's list and found that none of them was followed by a notable increase of the *Dst* index.

[47] Finally, we suppose to implement this algorithm into the RPW instrument on the Solar Orbiter mission [*Maksimovic et al.*, 2007]. These missions would encounter predominantly ICMEs generated fast (forward or reverse) shocks and occasionally planetary (fast reverse) bow shocks during Earth and Venus flybys scheduled for the orbital changes. We have shown that the suggested setting of algorithm parameters is appropriate for their identification. However, an additional effort could be required for optimization of the algorithm free parameters during onboard operations.

[48] **Acknowledgments.** The authors would like to thank J. C. Kasper for use of the Wind IP shock list. The authors acknowledge V. Krasnosel'skikh and M. Kretzschmar (CNRS, France) for their useful discussions on this work. The present work was supported by the Czech Grant Agency under Contracts 13-37174P, 205/09/0112, and P209/12/2207.

[49] Philippa Browning thanks Ian G. Richardson and another reviewer for their assistance in evaluating this paper.

References

de Lucas, A., R. Schwenn, A. Dal Lago, E. Marsch, and A. L. Clúa de Gonzalez (2011), Interplanetary shock wave extent in the inner heliosphere as observed by multiple spacecraft, *J. Atmos. Sol. Terr. Phys.*, *73*, 1281–1292, doi:10.1016/j.jastp.2010.12.011.

Echer, E., W. D. Gonzalez, and M. V. Alves (2006), On the geomagnetic effects of solar wind interplanetary magnetic structures, *Space Weather*, *4*, S06001, doi:10.1029/2005SW000200.

Echer, E., et al. (2003), Geomagnetic effects of interplanetary shock waves during solar minimum (1995–1996) and solar maximum (2000), in *Solar Variability as an Input to the Earth's Environment,* vol. 535, edited by A. Wilson, pp. 641–644, ESA Special Publication.

Galeev, A. A., S. I. Klimov, V. N. Lutsenko, S. Fischer, and K. Kudela (1986), Project intershock - Complex analysis of the bow shock crossing on 7 May 1985, *Adv. Space Res.*, *6*, 45–48, doi:10.1016/0273-1177(86)90008-6.

Gonzalez, W. D., J. A. Joselyn, Y. Kamide, H. W. Kroehl, G. Rostoker, B. T. Tsurutani, and V. M. Vasyliunas (1994), What is a geomagnetic storm?, *J. Geophys. Res.*, *99*, 5771–5792, doi:10.1029/93JA02867.

Gonzalez, W. D., B. T. Tsurutani, and A. L. Clúa de Gonzalez (1999), Interplanetary origin of geomagnetic storms, *Space Sci. Rev.*, *88*, 529–562, doi:10.1023/A:1005160129098.

Gosling, J. T., S. J. Bame, D. J. McComas, J. L. Phillips, E. E. Scime, V. J. Pizzo, B. E. Goldstein, and A. Balogh (1994), A forward-reverse shock pair in the solar wind driven by over-expanison of a coronal mass ejection: ULYSSES observations, *Geophys. Res. Lett.*, *21*, 237–240, doi:10.1029/94GL00001.

Ho, C. M., B. T. Tsurutani, N. Lin, L. J. Lanzerotti, E. J. Smith, B. E. Goldstein, B. Buti, G. S. Lakhina, and X. Y. Zhou (1998), A pair of forward and reverse slow-mode shocks detected by Ulysses at 5 AU, *Geophys. Res. Lett.*, *25*, 2613–2616, doi:10.1029/98GL02014.

Jian, L. K., C. T. Russell, J. G. Luhmann, and D. Curtis (2013), Burst Mode trigger of STEREO in situ measurement, in *American Institute of Physics Conference Series,* vol. 1539, edited by G.-P. Zank et al., pp. 195–198. doi:10.1063/1.4811021.

Joselyn, J. C., J. W. Hirman, and G. R. Heckman (1981), ISEE 3 in real time: An update, *EOS Transactions*, *62*, 617–618, doi:10.1029/EO062i032p00617.

Kartalev, M. D., K. G. Grigorov, Z. Smith, M. Dryer, C. D. Fry, W. Sun, and C. S. Deehr (2002), Comparative study of predicted and experimentally detected interplanetary shocks, in *Solspa 2001, Proceedings of the Second Solar Cycle and Space Weather Euroconference,* vol. 477, edited by H. Sawaya-Lacoste, pp. 355–358, ESA Special Publication.

Kennel, C. F., J. P. Edmiston, and T. Hada (1985), A quarter century of collisionless shock research, *Washington DC American Geophysical Union Geophysical Monograph Series*, *34*, 1–36.

Lepping, R. P., et al. (1995), The wind magnetic field investigation, *Space Sci. Rev.*, *71*, 207–229, doi:10.1007/BF00751330.

Lepping, R. P., et al. (2001), The bastille day magnetic clouds and upstream Shocks: Near-Earth interplanetary observations, *Sol. Phys.*, *204*, 285–303, doi:10.1023/A:1014264327855.

Lin, C. C., H. Q. Feng, D. J. Wu, J. K. Chao, L. C. Lee, and L. H. Lyu (2009), Two-spacecraft observations of an interplanetary slow shock, *J. Geophys. Res.*, *114*, A03105, doi:10.1029/2008JA013154.

Lin, R. P., et al. (1995), A three-dimensional plasma and energetic particle investigation for the wind spacecraft, *Space Sci. Rev.*, *71*, 125–153, doi:10.1007/BF00751328.

Lindsay, G. M., C. T. Russell, J. G. Luhmann, and P. Gazis (1994), On the sources of interplanetary shocks at 0.72 AU, *J. Geophys. Res.*, *99*, 11–17, doi:10.1029/93JA02666.

Luhmann, J. G. (1997), CMEs and space weather, *Washington DC American Geophysical Union Geophysical Monograph Series*, *99*, 291–299, doi:10.1029/GM099p0291.

Luhmann, J. G., et al. (2008), STEREO IMPACT investigation goals, measurements, and data products overview, *Space Sci. Rev.*, *136*, 117–184, doi:10.1007/s11214-007-9170-x.

Maksimovic, M., et al. (2007), A radio and plasma wave experiment for the Solar orbiter mission*, Proceedings of the 2nd Solar Orbiter Workshop,* 16 - 20 October 2006, Athens, Greece, ESA SP-641.

Manchester, W. B., and T. H. Zurbuchen (2006), Are high-latitude forward-reverse shock pairs driven by CME overexpansion?, *J. Geophys. Res.*, *111*, A05101, doi:10.1029/2005JA011461.

March, T. K., S. C. Chapman, and R. O. Dendy (2005), Mutual information between geomagnetic indices and the solar wind as seen by WIND: Implications for propagation time estimates, *Geophys. Res. Lett.*, *32*, L04101, doi:10.1029/2004GL021677.

McKenna-Lawlor, S. M. P., M. Dryer, M. D. Kartalev, Z. Smith, C. D. Fry, W. Sun, C. S. Deehr, K. Kecskemety, and K. Kudela (2006), Near real-time predictions of the arrival at Earth of flare-related shocks during Solar Cycle 23, *J. Geophys. Res.*, *111*, A11103, doi:10.1029/2005JA011162.

McKenna-Lawlor, S. M. P., C. D. Fry, M. Dryer, D. Heynderickx, K. Kecskemety, K. Kudela, and J. Balaz (2012), A statistical study of the performance of the Hakamada-Akasofu-Fry version 2 numerical model in predicting solar shock arrival times at Earth during different phases of solar cycle 23, *Ann. Geophys.*, *30*, 405–419, doi:10.5194/angeo-30-405-2012.

Müller, D., R. G. Marsden, O. C. St. Cyr, and H. R. Gilbert (2012), Solar orbiter, *Sol. Phys.*, doi:10.1007/s11207-012-0085-7.

Musmann, G., F. M. Neubauer, F. O. Gliem, and R. P. Kugel (1979), Shock-identification-computer on board of the spacecrafts Helios-1 and Helios-2, *IEEE Transactions on Geoscience Electronics*, *17*, 92–95.

Schwartz, S. J. (2006), Shocks: Commonalities in solar-terrestrial chains, *Space Sci. Rev.*, *124*, 333–344, doi:10.1007/s11214-006-9093-y.

Tóth, G., et al. (2005), Space Weather Modeling Framework: A new tool for the space science community, *J. Geophys. Res.*, *110*, A12226, doi:10.1029/2005JA011126.

Tsurutani, B. T., and W. D. Gonzalez (1998), Magnetic storms, in *From the Sun, Auroras, Magnetic Storms, Solar Flares, Cosmic Rays*, edited by S. T. Suess and B. T. Tsurutani, p. 57, AGU, Washington, D. C., doi:10.1029/SP050.

Tsurutani, B. T., and R. P. Lin (1985), Acceleration of greater than 47 keV ions and greater than 2 keV electrons by interplanetary shocks at 1 AU, *J. Geophys. Res.*, *90*, 1–11, doi:10.1029/JA090iA01p00001.

Tsurutani, B. T., E. J. Smith, W. D. Gonzalez, F. Tang, and S. I. Akasofu (1988), Origin of interplanetary southward magnetic fields responsible for major magnetic storms near solar maximum (1978–1979), *J. Geophys. Res.*, *93*, 8519–8531, doi:10.1029/JA093iA08p08519.

Tsurutani, B. T., Y. T. Lee, W. D. Gonzalez, and F. Tang (1992), Great magnetic storms, *Geophys. Res. Lett.*, *19*, 73–76, doi:10.1029/91GL02783.

Tsurutani, B. T., G. S. Lakhina, O. P. Verkhoglyadova, W. D. Gonzalez, E. Echer, and F. L. Guarnieri (2011), A review of interplanetary discontinuities and their geomagnetic effects, *J. Atmos. Sol. Terr. Phys.*, *73*, 5–19, doi:10.1016/j.jastp.2010.04.001.

Tsurutani, B. T., et al. (2006), Corotating solar wind streams and recurrent geomagnetic activity: A review, *J. Geophys. Res.*, *111*, A07S01, doi:10.1029/2005JA011273.

Vandev, D., K. Danov, P. Mateev, P. Petrov, and M. Kartalev (1986), Development of a real-time algorithm for detection of solar wind discontinuities, *Astrophys. Space Sci.*, *120*, 211–221, doi:10.1007/BF00649937.

Vorotnikov, V. S., C. W. Smith, Q. Hu, A. Szabo, R. M. Skoug, and C. M. S. Cohen (2008), Automated shock detection and analysis algorithm for space weather application, *Space Weather*, *6*, S03002, doi:10.1029/2007SW000358.

Vorotnikov, V. S., et al. (2011), Use of single-component wind speed in Rankine-Hugoniot analysis of interplanetary shocks, *Space Weather*, *9*, S04001, doi:10.1029/2010SW000631.

Watari, S., and T. Watanabe (1998), The solar drivers of geomagnetic disturbances during solar minimum, *Geophys. Res. Lett.*, *25*, 2489–2492, doi:10.1029/98GL01085.

Zastenker, G. N., M. O. Riazantseva, and P. E. Eiges (2006), Multipoint observations of sharp boundaries of solar wind density structures, *Cosmic Res.*, *44*, 493–499, doi:10.1134/S0010952506060050.

Zhou, X., and B. T. Tsurutani (2001), Interplanetary shock triggering of nightside geomagnetic activity: Substorms, pseudobreakups, and quiescent events, *J. Geophys. Res.*, *106*, 18,957–18,968, doi:10.1029/2000JA003028.